INTERNATIONAL JOURNAL FOR NUMERICAL METHODS IN FLUIDS, VOL. 15, 1383–1406 (1992)

ON A NETWORK METHOD FOR UNSTEADY INCOMPRESSIBLE FLUID FLOW ON TRIANGULAR GRIDS

C. A. HALL AND T. A. PORSCHING

Department of Mathematics and Statistics, University of Pittsburgh, Pittsburgh, PA 15260, U.S.A.

AND

G. L. MESINA

EG&G, Idaho National Engineering Laboratory, Idaho Falls, ID 83415, U.S.A.

SUMMARY

The dual variable method for Delaunay triangulations is a network-theoretic method that transforms a set of primitive variable finite difference or finite element equations for incompressible flow into an equivalent system which is one-fifth the size of the original. Additionally, it eliminates the pressures from the system and produces velocities that are exactly discretely divergence-free. In this paper new discretizations of the convection term are presented for Delaunay triangulations, the dual variable method is extended to tessellations that contain obstacles, and an efficient algorithm for the solution of the dual variable system is described.

KEY WORDS Incompressible flow Co-volume method Upwind Voronoi tessellation Networks

1. INTRODUCTION

Techniques for generating finite-difference-like representations of the equations of fluid dynamics on non-rectangular grids were presented in References 1 and 2. In subsequent works[3–7] special attention was paid to triangular grids, which are the subject of this paper. The basic idea in this work, which is a generalization of the concepts used in the MAC method[8] for rectangular grids, is to develop finite-dimensional analogs of the continuity and momentum equations by considering complementary or co-volume decompositions of the flow domain.

In the two-dimensional case, if the continuity equation is discretized on triangular cells, then the 'natural' complementary cells for the momentum equation are the so-called Voronoi polygons.[9] It is somewhat remarkable that such a general method admits a simple network- (or graph-) theoretic interpretation. The sides (links) and vertices (nodes) of the Voronoi polygons form a directed network $\mathbf{N}$, while those of the triangles constitute its dual $\mathbf{N}^*$.[2] Each link of $\mathbf{N}$ carries a flow that is an approximation of the normal mass flux across one of the triangle's sides, and each node of $\mathbf{N}$ carries a state that is an approximation of the pressure in one of the triangles. The states and flows on $\mathbf{N}$ are determined by a system of node laws and link characteristics obtained, respectively, from the continuity and momentum equations.

To be more specific, suppose that the triangulated flow region comprises N triangles having L interior sides. Let $\mathbf{n}_j$, $j=1, \ldots, L$, denote a unit normal vector to the jth side, let h_j denote the length of side j, and let $\mathbf{q}_j$ be an approximation to the midside velocity vector. If we assume for

0271–2091/92/241383–24$17.00

Received 14 June 1991
Revised 22 June 1992

simplicity that the boundary conditions are homogeneous (the treatment of inhomogeneous boundary conditions is briefly discussed in Section 3; see Reference 4 for a more complete discussion), then the (spatially) discrete continuity equation on triangle i is

$$\sum_j a_{ij}\phi_j = 0, \quad i = 1, \ldots, N, \tag{1}$$

where $\phi_j = h_j \mathbf{q}_j \cdot \mathbf{n}_j$ is the normal mass flux across side j, and

$$a_{ij} = \begin{cases} 1 & \text{if } \mathbf{n}_j \text{ is the outward normal of side } j, \\ -1 & \text{if } \mathbf{n}_j \text{ is the inward normal of side } j, \\ 0 & \text{otherwise.} \end{cases}$$

The vector $\mathbf{n}_j$ defines the direction and sense of the jth link in $\mathbf{N}$. In this context the matrix $A = [a_{ij}] \in R^{N \times L}$ is actually the incidence matrix of $\mathbf{N}$, and equations (1) are its node laws. If we let ξ_j denote the normal velocity component on side j, i.e. $\xi_j = \mathbf{q}_j \cdot \mathbf{n}_j$, with $\xi = (\xi_1, \ldots, \xi_L)^{\mathrm{T}}$ and $H = \operatorname{diag}(h_j) \in R^{L \times L}$, then (1) can be written as

$$AH\xi = 0. \tag{2}$$

If the (unsteady) momentum equation is appropriately semi-discretized at the midpoints of interior triangle sides, it gives rise to a set of L ordinary differential equations whose vector form is

$$\frac{\mathrm{d}\xi}{\mathrm{d}t} + M(\xi)\xi = G^{-1}A^{\mathrm{T}}\mathbf{p} + \mathbf{b}. \tag{3}$$

Here $\mathbf{p} \in R^N$ is a vector of discrete pressures associated with the triangle interiors and $\mathbf{b} \in R^L$ is a discrete body force. The matrix $G^{-1} = \operatorname{diag}(1/h_j') \in R^{L \times L}$, where h_j' is the length of the jth link of $\mathbf{N}$ (i.e. the jth Voronoi side). Finally, the matrix $M(\xi) \in R^{L \times L}$ accounts for the discretization of the convection and viscous terms. In network terminology equation (3) constitutes the link characteristics of $\mathbf{N}$. Taken together with the node laws of (2), they determine the unknown vectors ξ and $\mathbf{p}$.

Once the above identifications have been made, the dual variable method[11,12] (see also References 13 and 14) is applicable. The dual variables are states on the nodes of $\mathbf{N}^*$, i.e. the vertices of the triangles. If the flow region is simply connected, then the boundaries of the Voronoi polygons form a basis of elementary cycles for $\mathbf{N}$ and an *exact* representation of the most general flows satisfying the node laws can be given in terms of the dual variables. Moreover, a transformation of the link characteristics then produces a closed system that determines the dual variables.

The specific application of these ideas to the system described by equations (2) and (3) proceeds as follows. The dimension of the elementary cycle basis is known to be $L - N + 1$, and each cycle gives a simple prescription for the determination of a linearly independent vector in $\ker A$. Thus, $\dim \ker A = L - N + 1$, and using the elementary cycles of $\mathbf{N}$, it is straightforward to construct a fundamental matrix $C \in R^{L \times (L-N+1)}$ whose columns form a basis for $\ker A$. If we let $\mathbf{U} = H\xi$, then by (2), $\mathbf{U} = C\gamma$ for some vector of dual variables, $\gamma \in R^{L-N+1}$. Thus, $\xi = H^{-1}C\gamma$ and it follows from (3) that

$$GH^{-1}C\frac{\mathrm{d}\gamma}{\mathrm{d}t} + GM(H^{-1}C\gamma)H^{-1}C\gamma = A^{\mathrm{T}}\mathbf{p} + G\mathbf{b}. \tag{4}$$

Multiplying (4) by C^{T} and observing that $C^{\mathrm{T}}A^{\mathrm{T}} = (AC)^{\mathrm{T}} = 0$, we obtain

$$C^{\mathrm{T}}GH^{-1}C\frac{\mathrm{d}\gamma}{\mathrm{d}t} + C^{\mathrm{T}}GM(H^{-1}C\gamma)H^{-1}C\gamma = C^{\mathrm{T}}G\mathbf{b}, \tag{5}$$

which is a system of ordinary differential equation of order $L-N+1$ for γ. Since the matrix $C^{\mathrm{T}}GH^{-1}C$ is symmetric positive-definite, (5) represents a well-posed initial value problem for γ provided that the initial velocity field satisfies the discrete divergence-free condition $H\xi(0)\in\ker A$.

There are several reasons for working with the dual rather than the primitive variables. For example:

(1) The semi-discrete dual variable system [equation (5)] is a standard ordinary differential equation system, whereas the semidiscrete primitive variable system [equations (2) and (3)] is a differential–algebraic equation system incorporating both differential equations and algebraic constraints.
(2) After total (space and time) discretization, the size of the dual variable system is about *one-fifth* the size of the primitive system. It is important to note that this reduction factor is preserved even when the convection and viscous terms in the momentum equation are treated *implicitly*. This reduction is not the result of any further approximation of the primitive system; indeed, there is a one-to-one correspondence between the solutions of the primitive system and those of the dual variable system. Rather, the reduction is due to the exact represenation of the link flows as a coset with respect to a subspace whose dimension is about one-fifth that of the discrete velocity and pressure spaces.
(3) Discrete mass is automatically conserved on the triangular cells and the degree of conservation is essentially independent of the accuracy of the solution of the dual variable system.
(4) The discrete pressures are completely eliminated from the computations. However, they can be easily recovered if desired.

This paper should be considered a sequel to Reference 4. Consequently, we will assume a general familiarity with the notions and terminology of that work. Our goal here is to generalize the results of Reference 4 in three respects. First, we develop several new discretizations of the non-linear convection term in the momentum equation. One of these may be interpreted as a generalized centred difference scheme, while another is more properly termed an upwind method. The (semi)implicit versions of these schemes are of speical interest since they relieve the familiar restrictions on the time-step size that are necessary for stability when the schemes are used in their explicit forms. We emphasize again that the additional couplings introduced by an implicit discretization of the convection (or viscous) term have *no* effect on the features of the dual variable method mentioned above. In particular, the size reduction factor of five still applies! We know of no other computational fluid dynamics method with this property. Second, we describe the modifications that are necessary in the dual variable method to accommodate multiply connected flow regions. This allows us to treat problems with embedded solids. Third, we analyse the structure of the dual variable system and describe a special algorithm for its solution. Finally, we illustrate these features with a series of numerical examples.

2. CONVECTION TERM DISCRETIZATIONS

In this section we develop discretizations of the convection term in the momentum equation that on triangular grids are analogs of the usual centred and upwind schemes. These provide alternatives to the one presented in Reference 4, which, as we illustrate below, produces unstable results for rather modest-sized time steps.

Recall that the time-dependent momentum equation can be written as

$$\mathbf{q}_t+\nabla\cdot(\mathbf{q}\mathbf{q}^{\mathrm{T}})-\nu\nabla^2\mathbf{q}=-\nabla p+\mathbf{f}, \tag{6}$$

where $\mathbf{q}$ is the divergence-free velocity vector, ν is the kinematic viscosity, p and $\mathbf{f}$ are the (reduced) pressure and body force, $\nabla\cdot$ is the divergence operator, $\mathbf{q}\mathbf{q}^{\mathrm{T}}$ is a dyadic product, ∇^2 is the Laplacian, and ∇ is the gradient operator. To put this equation in a form more suitable for discretization on a triangular grid, we let $\mathbf{r}$ be a constant unit vector and take the dot product of the momentum equation (6) with $\mathbf{r}$.

For the viscous stress term, let ω denote the *scalar* vorticity as given by Peyret and Taylor (Reference 17, p. 16). Then, since $\nabla\cdot\mathbf{q}=0$, it can be shown that

$$-(\nabla^2\mathbf{q})\cdot\mathbf{r}=\frac{\partial\omega}{\partial s}, \tag{7}$$

where $\partial/\partial s$ denotes differentiation in the direction of $\mathbf{s}$, the unit vector orthogonal to $\mathbf{r}$ such that $\mathbf{r}, \mathbf{s}$ form a right-handed system.*

Now consider the convection term. By again making use of the incompressibility condition $\nabla\cdot\mathbf{q}=0$, we can verify the identity

$$[\nabla\cdot(\mathbf{q}\mathbf{q}^{\mathrm{T}})]\cdot\mathbf{r}=[\nabla(\mathbf{q}\cdot\mathbf{r})]\cdot\mathbf{q}.$$

It follows that if $\mathbf{q}\neq 0$, then

$$[\nabla\cdot(\mathbf{q}\mathbf{q}^{\mathrm{T}})]\cdot\mathbf{r}=\left[\frac{\partial}{\partial q}(\mathbf{q}\cdot\mathbf{r})\right]|\mathbf{q}|, \tag{8}$$

where $\partial/\partial q$ denotes the directional derivative in the direction of $\mathbf{q}$ and $|\mathbf{q}|$ is its Euclidean length. Since also $\nabla p\cdot\mathbf{r}=\partial p/\partial r$, the directional derivative of p in the direction $\mathbf{r}$, the form of (6) to be discretized is the scalar equation

$$\mathbf{q}_t\cdot\mathbf{r}+\left[\frac{\partial}{\partial q}(\mathbf{q}\cdot\mathbf{r})\right]|\mathbf{q}|+\nu\frac{\partial\omega}{\partial s}=-\frac{\partial p}{\partial r}+\mathbf{f}\cdot\mathbf{r}. \tag{9}$$

All terms other than the convection term are now treated as in Reference 4. For example, the directional derivative given by (7) is discretized at the midpoint of a typical side of the triangular grid by choosing $\mathbf{r}$ to be a unit normal to that side and approximating the values of ω at the side's vertices. The approximations involve the use of Green's theorem and ultimately yield an expression in terms of the velocity components that are normal to the sides of the triangles. See Reference 4 for details.

As in the case of the viscous stress term, we are interested in approximating the right-hand side of (8) at P, the midpoint of a typical interior side of the triangular grid when $\mathbf{r}=\mathbf{n}_P$, a unit normal to that side. Suppose that $\mathbf{q}_P$ is an approximation of $\mathbf{q}(P)$, the velocity at P. As shown in Figure 1, let two triangles share the side containing P, and let Q' and R' denote the points of intersection of the line through P in the direction of $\mathbf{q}_P$ with the boundaries of these triangles. As our 'centred' approximation at P, we take

$$\left\{\frac{\partial}{\partial q}[\mathbf{q}(P)\cdot\mathbf{n}_P]\right\}|\mathbf{q}(P)|\approx\pm\frac{\mathbf{q}_{R'}\cdot\mathbf{n}_P-\mathbf{q}_{Q'}\cdot\mathbf{n}_P}{|R'-Q'|}|\mathbf{q}_P|, \tag{10}$$

where $\mathbf{q}_{R'}$ and $\mathbf{q}_{Q'}$ are the analogs of $\mathbf{q}_P$ at R' and Q' and the plus or minus sign is used as $\mathbf{q}_P\cdot\mathbf{n}_P\geq 0$

* By this we mean that $\mathbf{s}$ is obtained by rotating $\mathbf{r}$ in the counterclockwise direction by 90°.

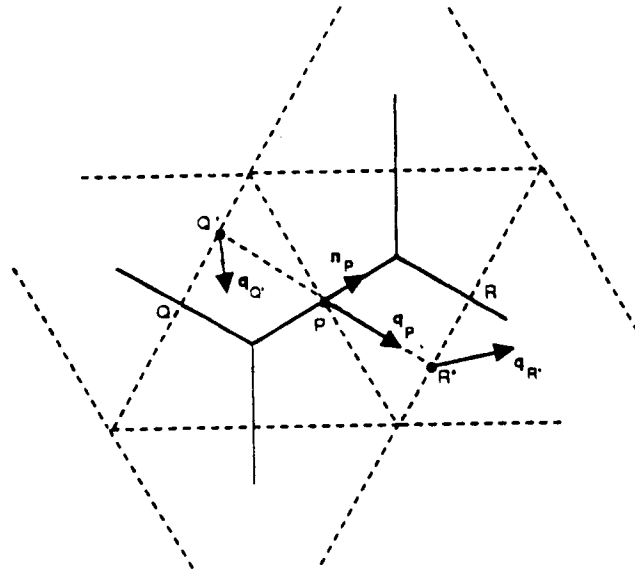

Figure 1. A triangular grid showing a portion of the complementary Voronoi polygons (solid lines)

or not. The 'upwind' approximation is given by

$$\left\{\frac{\partial}{\partial q}[\mathbf{q}(P)\cdot\mathbf{n}_P]\right\}|\mathbf{q}(P)| \approx \begin{cases} \dfrac{\mathbf{q}_P\cdot\mathbf{n}_P-\mathbf{q}_{Q'}\cdot\mathbf{n}_P}{|P-Q'|}|\mathbf{q}_P| & \text{if } \mathbf{q}_P\cdot\mathbf{n}_P\geq 0, \\ \dfrac{\mathbf{q}_P\cdot\mathbf{n}_P-\mathbf{q}_{R'}\cdot\mathbf{n}_P}{|P-R'|}|\mathbf{q}_P| & \text{if } \mathbf{q}_P\cdot\mathbf{n}_P<0. \end{cases} \tag{11}$$

It is clear that (11) follows the usual upwind prescription for differencing a directional derivative. It remains to express the schemes given by (10) and (11) solely in terms of the velocity components that are normal to the sides of the triangles since, as we have seen, these (and the discrete pressures) are the fundamental primitive variables.

We begin by replacing $\mathbf{q}_{Q'}$ and $\mathbf{q}_{R'}$ by the corresponding midside velocities $\mathbf{q}_Q$ and $\mathbf{q}_R$ (see Figure 1). This falsifies the numerators in (10) and (11) by an amount that is proportional to the grid gage h. Since the denominators are also of the order of h, the resulting difference approximation is not consistent in the classical sense. However, we choose to interpret the differences in (10) and (11) as differences of averages of flows across respective triangle sides in the direction $\mathbf{n}_P$. As such, $\mathbf{q}\cdot\mathbf{n}_P$ is assumed constant along each side of the triangle, and the above substitutions are consistent with this point of view. Furthermore, the only error analysis of which we are aware for co-volume methods[15,16] does not follow the classical pointwise finite difference error analyses; instead, the approach is more like a finite element analysis using an area or L_2 norm. So, it is not clear that one should expect pointwise consistency in the context of co-volume approaches. The authors will report elsewhere on a pointwise consistent upwind scheme for triangular meshes. We remark that such a method is considerably more complex and computationally costly than the one presented here.

Numerical experimentation (see e.g. Section 6) indicates that the approximations made above to (10) and (11) do not destroy convergence (in the proper choice of norm) as the mesh gage

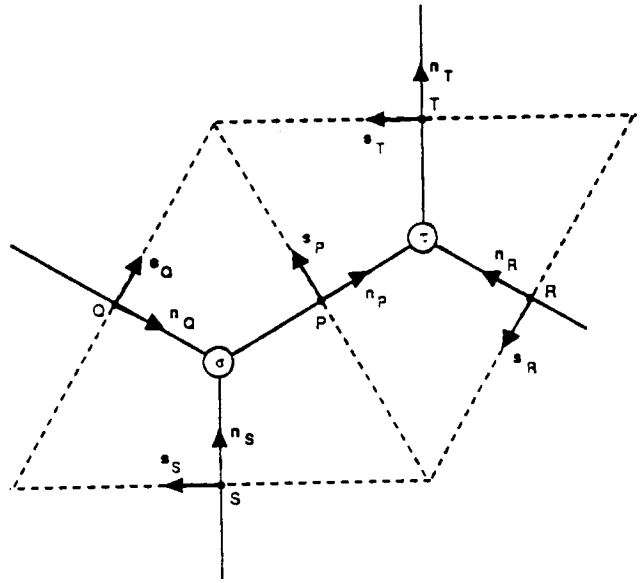

Figure 2. Local co-ordinate systems

decreases. In fact, for the results given in Section 6 as well as other numerical experimentation, the replacement of $\mathbf{q}_{Q'}$ and $\mathbf{q}_{R'}$ by the corresponding midside velocities $\mathbf{q}_Q$ and $\mathbf{q}_R$ produces steady-state solutions which are about as accurate as those produced using the schemes presented in References 4 and 7. In addition, the upwind scheme used here is more robust and appears to be unconditionally stable.

The problem now is to represent the midside velocity vectors $\mathbf{q}_P$, $\mathbf{q}_Q$, etc., in terms of the normal velocity components ξ_P, ξ_Q, etc. We first construct the velocities $\mathbf{q}_\sigma$ and $\mathbf{q}_\tau$ at the two Voronoi vertices σ and τ shown in Figure 2 (recall that these are also nodes of the network $\mathbf{N}$). These velocities are then used in formula (16) below to define the midside velocity $\mathbf{q}_P$.

With reference to Figure 2, we let $(\mathbf{n}_P, \mathbf{s}_P)$, $(\mathbf{n}_Q, \mathbf{s}_Q)$, etc., denote unit normal–tangent vector pairs to sides P, Q, etc. The sense of each unit normal vector is determined by the direction of the link on which it lies, and the sense of the corresponding unit tangent vector is such that the pair forms a right-handed system.

Consider the triangle associated with the vertex σ and let $\mathbf{q}'_P$, $\mathbf{q}'_Q$, $\mathbf{q}'_S$ be provisional† midside velocities at P, Q, S, respectively. We define a velocity vector at σ as the barycentric interpolant on triangle PQS of the velocities $\mathbf{q}'_P$, $\mathbf{q}'_Q$ and $\mathbf{q}'_S$, i.e.

$$\mathbf{q}_\sigma = \theta_P \mathbf{q}'_P + \theta_Q \mathbf{q}'_Q + \theta_S \mathbf{q}'_S, \tag{12}$$

where $\theta_P = \text{Area}(\Delta\sigma QS)/\text{Area}(\Delta PQS)$, etc., and where

$$\begin{aligned} \mathbf{q}'_P &= \xi_P \mathbf{n}_P + \eta'_P \mathbf{s}_P, \\ \mathbf{q}'_Q &= \xi_Q \mathbf{n}_Q + \eta'_Q \mathbf{s}_Q, \\ \mathbf{q}'_S &= \xi_S \mathbf{n}_S + \eta'_S \mathbf{s}_S. \end{aligned} \tag{13}$$

† These quantities depend on information only from the triangle associated with σ, whereas the definition of $\mathbf{q}_P$, for example, also incorporates information from the triangle associated with τ.

The tangential components η'_P, η'_Q, η'_S will now be determined. (We remark that in Reference 4, $\mathbf{q}_\sigma$ was taken to be the average of $\mathbf{q}'_P$, $\mathbf{q}'_Q$ and $\mathbf{q}'_S$, i.e. $\theta_P=\theta_Q=\theta_S\equiv 1/3$. As such, $\mathbf{q}_\sigma$ is independent of the location of σ.)

Following Reference 4, we determine η'_P, η'_Q and η'_S as functions of the quantities ξ_P, ξ_Q and ξ_S by requiring that

$$\mathbf{q}_\sigma\cdot\mathbf{s}_P=\eta'_P,\qquad \mathbf{q}_\sigma\cdot\mathbf{s}_Q=\eta'_Q \quad\text{and}\quad \mathbf{q}_\sigma\cdot\mathbf{s}_S=\eta'_S. \tag{14}$$

Substituting (12) and (13) into (14), we obtain the linear system

$$A\boldsymbol{\eta}'=B\boldsymbol{\xi}, \tag{15}$$

where $\boldsymbol{\eta}'=(\eta'_P,\eta'_Q,\eta'_S)^{\mathrm{T}}$, $\boldsymbol{\xi}=(\xi_P,\xi_Q,\xi_S)^{\mathrm{T}}$,

$$A=\begin{bmatrix} 1-\theta_P & -\theta_Q\mathbf{s}_Q\cdot\mathbf{s}_P & -\theta_S\mathbf{s}_S\cdot\mathbf{s}_P \\ -\theta_P\mathbf{s}_P\cdot\mathbf{s}_Q & 1-\theta_Q & -\theta_S\mathbf{s}_S\cdot\mathbf{s}_Q \\ -\theta_P\mathbf{s}_P\cdot\mathbf{s}_S & -\theta_Q\mathbf{s}_Q\cdot\mathbf{s}_S & 1-\theta_S \end{bmatrix},$$

and

$$B=\begin{bmatrix} 0 & \theta_Q\mathbf{n}_Q\cdot\mathbf{s}_P & \theta_S\mathbf{n}_S\cdot\mathbf{s}_P \\ \theta_P\mathbf{n}_P\cdot\mathbf{s}_Q & 0 & \theta_S\mathbf{n}_S\cdot\mathbf{s}_Q \\ \theta_P\mathbf{n}_P\cdot\mathbf{s}_S & \theta_Q\mathbf{n}_Q\cdot\mathbf{s}_S & 0 \end{bmatrix}.$$

Observe that the matrix A is strictly diagonally dominant; so, (15) uniquely determines $\boldsymbol{\eta}'$ in terms of $\boldsymbol{\xi}$.

We compute $\mathbf{q}_\tau$ at the Voronoi vertex τ in a similar manner. Then we take

$$\mathbf{q}_P=\xi_P\mathbf{n}_P+\eta_P\mathbf{s}_P, \tag{16}$$

where

$$\eta_P=\frac{|P-\tau|\,\mathbf{q}_\sigma\cdot\mathbf{s}_P+|P-\sigma|\,\mathbf{q}_\tau\cdot\mathbf{s}_P}{|\sigma-\tau|}. \tag{17}$$

In Reference 4, the weights in (17) were set equal to 1/2, i.e. an arithmetic average was used. This is also the scheme used in the numerical examples of Section 6. If one or more of the points Q, R, S, T lies on a boundary of the flow region, then we proceed in a somewhat different manner. We assume that the normal and tangential velocity components are known at such points.‡ Suppose for definiteness that Q lies on a boundary and that ξ^*_Q, η^*_Q are the known normal and tangential components. Then the second equation of (13) is replaced by

$$\mathbf{q}'_Q=\xi^*_Q\mathbf{n}_Q+\eta^*_Q\mathbf{s}_Q,$$

and the second equation of (14) is not used.

Finally, if the point P itself lies on a boundary, then the procedure reduces to replacing (16) by

$$\mathbf{q}_P=\xi^*_P\mathbf{n}_P+\eta^*_P\mathbf{s}_P,$$

where ξ^*_P and η^*_P are the known velocity components.

‡ That is, we assume that (consistent) normal boundary fluxes are specified on the boundary of the flow region. If pressures are included as part of the boundary conditions, then the subsequent discussion requires a slight modification. However, the conclusions remain unchanged.

3. MULTIPLY CONNECTED REGIONS

In Reference 4 the dual variable method was applied to triangular grids on flow regions free of obstacles. As mentioned in the introduction, in this case we can represent the class of discretely divergence-free flows on the triangular cells as a co-set with respect to the subspace of elementary cycles of **N**. More specifically, let L be the number of links of **N** (i.e. the number of sides of the Voronoi polygons). Then the most general divergence free L-dimensional flow vector $\boldsymbol{\phi}$ that satisfies the (non)homogeneous boundary conditions has the representation

$$\boldsymbol{\phi}=\boldsymbol{\phi}_0+\boldsymbol{\psi}. \tag{18}$$

Here $\boldsymbol{\phi}_0$ is any *particular* such vector and $\boldsymbol{\psi}$ is divergence-free, zero on the boundary, and lies in a subspace of dimension $L-N+1$, where N is the number of nodes of **N** (i.e. the number of Voronoi vertices).

It turns out that a basis for this subspace consists of vectors constructed from the elementary cycles of **N** defined by the boundaries of the Voronoi polygons (see Reference 4). At each interior node of **N**, i.e. a Voronoi vertex that is not associated with a triangle having a part of the boundary as one of its sides, the corresponding vector is *itself* divergence-free.

To illustrate this last point, consider Δabc, the triangle with vertices a, b, c shown in Figure 3. (cf. also Figure 2). Let the associated node σ be an interior node. If $\mathbf{q}$ is the velocity field and $\mathbf{n}$ a unit outward normal to ∂abc, the boundary of triangle abc, then, since $\nabla\cdot\mathbf{q}=0$,

$$0=\int_{\Delta abc}\nabla\cdot\mathbf{q}\,dA=\int_{\partial abc}\mathbf{q}\cdot\mathbf{n}\,ds\approx h_P\mathbf{q}_P\cdot\mathbf{n}_P-h_Q\mathbf{q}_Q\cdot\mathbf{n}_Q-h_S\mathbf{q}_S\cdot\mathbf{n}_S, \tag{19}$$

where $\mathbf{n}_P$, $\mathbf{q}_P$, etc., have been previously defined and h_P, h_Q and h_S are the side lengths of Δabc. In view of (19), we define the discrete continuity equation at node σ as

$$\phi_P-\phi_Q-\phi_S=0, \tag{20}$$

where $\phi_P\equiv h_P\mathbf{q}_P\cdot\mathbf{n}_P$, etc.; cf. equation (1).

The three cycles of **N** that share σ correspond to vertices a, b and c. Figure 3 shows only those portions of the cycles that affect the flows at node σ. The cycle basis vector at vertex a produces flows $\phi_P=0$, $\phi_Q=-1$ and $\phi_S=1$, while at vertices b and c the basis vectors yield $\phi_P=-1$, $\phi_Q=0$, $\phi_S=-1$ and $\phi_P=1$, $\phi_Q=1$, $\phi_S=0$, respectively. Clearly, each of these flow sets satisfy (20). All other cycle basis vectors generate the trivial flow set $\phi_P=\phi_Q=\phi_S=0$.

Regarding the vector $\boldsymbol{\psi}$, it follows from the prescription for the construction of the cycle basis that if ψ_P, ψ_Q and ψ_S are the components of $\boldsymbol{\psi}$ corresponding to links P, Q and S, then

$$\psi_P=-\gamma_b+\gamma_c,\qquad \psi_Q=\gamma_c-\gamma_a \quad\text{and}\quad \psi_S=\gamma_a-\gamma_b.$$

where γ_a, γ_b and γ_c are arbitrary states on the vertices a, b and c (i.e. dual variables on the nodes of **N***). Thus, we also have

$$\psi_P-\psi_Q-\psi_S\equiv 0,$$

which is consistent with (20) and the definition of $\boldsymbol{\psi}$ in (18), i.e. $\boldsymbol{\psi}$ is divergence-free.

Now suppose that the flow region is multiply connected due to the presence of obstacles or embedded solids. Although relation (18) remains true and the dimension of the subspace containing $\boldsymbol{\psi}$ is still $L-N+1$, the basis vectors provided by the Voronoi boundaries no longer span it. In fact, if the boundary of the flow region has $K+1$ components because of K interior obstacles, then K additional vectors are needed to complete the basis.

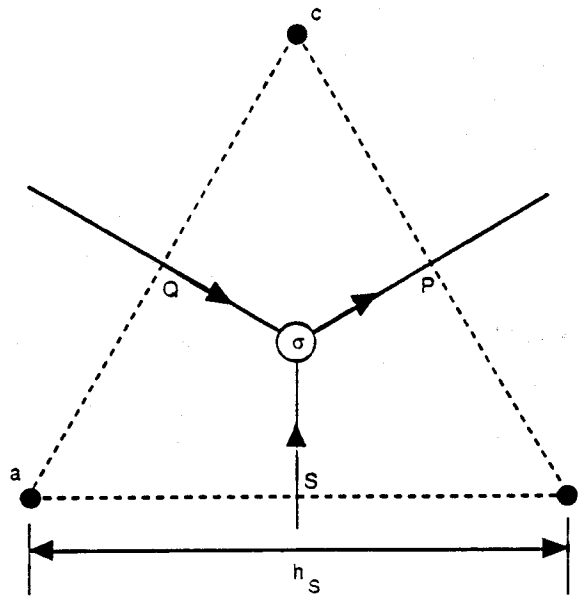

Figure 3. An interior node of N

To obtain these vectors we observe that if the Voronoi boundaries are used to construct the links of N in the usual way, then each interior boundary component of the flow region is itself surrounded by a closed contour of such links (see Figure 4). This means that the interiors of these contours along with the interiors of the Voronoi polygons constitute the *faces* of the planar network N. But it is known[10] that for planar networks the contours of the faces form a basis of cycles. Thus, the procedure that was used to produce the basis vectors in the simply connected case can again be used when the flow region is multiply connected. The difference is that there are now K 'exceptional' cycles corresponding to the contours surrounding the interior boundary components. We remark that an analogous result was given in Reference 14 and used in the determination of the dimension of a particular divergence-free finite element space.

We illustrate these ideas by considering the chevron-shaped obstacle of Figure 4. The surrounding contour consists of 22 directed links of N. It generates a basis vector with exactly 22 non-zero entries corresponding to the links of the contour. Each such entry is either $+1$ or -1 depending upon whether the link is directed with or against the sense of a traverse of the contour. If, for example, we choose to traverse the contour in the counterclockwise direction, then the entry corresponding to link P is $+1$, whereas that corresponding to link Q is -1.

The number of non-zero entries in a basis vector corresponding to a cycle defined by a Voronoi polygon is equal to the number of triangles that share the vertex associated with the cycle. If the grid consists only of equilateral triangles, then these vectors have exactly six non-zero entries (since the Voronoi polygon is a regular hexagon). This observation also applies (in an approximate sense) to a grid produced by a Delaunay triangulation of the flow region since then the resulting triangles are close to equilateral (see References 18 and 4). In this case it follows that, under a proper ordering, that part of the coefficient matrix of the dual variable system generated by these basis vectors is sparse and banded.

On the other hand, as we have just seen, the number of non-zero entries in the basis vector of an exceptional cycle equals the number of links that surround the boundary component, and this

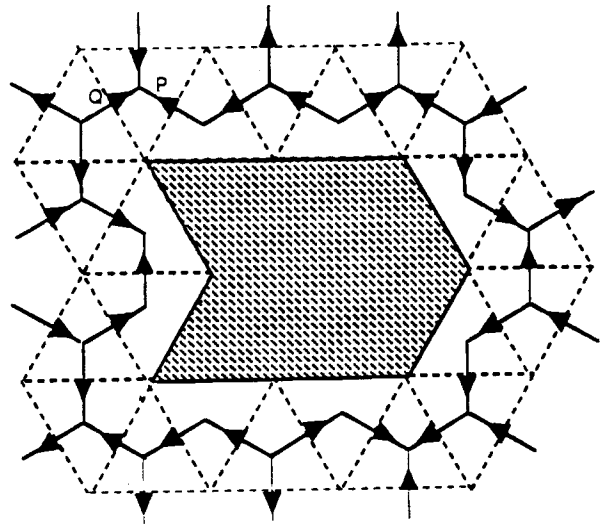

Figure 4. Obstacle and surrounding contour of links

could be quite large. Consequently, the presence of obstacles in the flow region has the potential to destroy the sparse banded structure of the dual variable coefficient matrix. However, it is reasonable to expect that the number of such obstacles (and corresponding exceptional cycles) is small relative to the total number of cycles in **N**. Assuming this to be the case, we see that with the proper ordering of cycles the coefficient matrix assumes a special *block* form. Accordingly, we next turn to a discussion of a block elimination method for such systems.§

4. BLOCK SYSTEMS

The dual variable linear system is of the form,[4]

$$C^{T}QC\gamma=\mathbf{b},$$

where C is the fundamental matrix of cycle vectors, Q is a matrix arising from the discrete momentum equations, γ is the vector of dual variables, and $\mathbf{b}$ is the source term. The coefficient matrix is non-symmetric and sparse. For problems which have flow regions with no obstacles, the coefficient matrix has a *skyline* (also called *profile*, *envelope*, or *variable band*) structure[20] which is confined to a narrow band. However, as noted in Section 3, the introduction of obstacles into the flow region produces exceptional cycles that generate non-zero entries falling outside this band; these are called *outriggers*. Outriggers represent couplings between a dual variable associated with a Voronoi polygon and one associated with an exceptional cycle. The number of non-zero entries in a row or column corresponding to the basis vector associated with an exceptional cycle depends on the size of the exceptional cycle; such a row or column may be nearly full. This dramatically increases the bandwidth and reduces the efficiency of standard banded- or full-matrix solvers.

§ One might also consider the use of a penalty method to deal with this problem (see e.g. Reference 19).

If the dual variables associated with the exceptional cycles are numbered last, the outriggers appear in the last rows and columns of the matrix. Such a matrix has a block 2×2 structure

$$B \equiv C^{\mathrm{T}} Q C = \begin{bmatrix} B_{11} & B_{12} \\ B_{21} & B_{22} \end{bmatrix},$$

where B_{11} is a square sparse matrix of skyline structure and B_{22} is a square (dense) matrix whose order is equal to the number of exceptional cycles. Figure 5 shows plots of the non-zero entries of typical matrices B. The first corresponds to the mesh containing 1016 triangles for the driven cavity flow problem and the second is for the mesh of 2252 triangles used for the nozzle problem considered in Section 6. Note that there are outriggers in the border (when obstacles are present), that B_{11} is of skyline structure and that all the non-zero entries fall within a relatively small bandwidth. Also, while B is *not* symmetric, it is *symmetrically non-zero.*

Since standard full- and banded-matrix solvers fail to take full advantage of the structure and sparseness pattern of the dual variable system, we considered specialized methods. Both the TR[21,22] and bordered-banded methods[23] were employed to solve the dual variable system; the latter performing somewhat better. However, the following method proved to be the most efficient.

If we compatibly partition γ and $\mathbf{b}$ as $(\gamma_1, \gamma_2)^{\mathrm{T}}$ and $(\mathbf{b}_1, \mathbf{b}_2)^{\mathrm{T}}$, then we can solve the dual variable system by first solving a skyline system with multiple right-hand sides. That is, we solve

$$B_{11}[Y \mid \mathbf{y}] = [B_{12} \mid \mathbf{b}_1] \tag{21}$$

for the matrix Y and vector $\mathbf{y}$. Next, we solve the dense (low-order) system

$$[B_{22} - B_{21} Y] \gamma_2 = \mathbf{b}_2 - B_{21} \mathbf{y}$$

for γ_2 and then recover γ_1 from the equation

$$\gamma_1 = \mathbf{y} - Y \gamma_2.$$

In the solution of (21), we take special cognizance of the zero–non-zero patterns in B_{11}. The solution is carried out with a specially designed skyline solver which does no elimination on rows corresponding to zero multipliers and reduces only the columns with indices between those designating the first and last non-zero entries in the pivot row.

5. TEMPORAL DISCRETIZATIONS OF THE CONVECTION TERM

In Section 2 we presented several spatial approximations of the convection term $\nabla \cdot (\mathbf{q}\mathbf{q}^{\mathrm{T}})$ in the momentum equation (6). To complete this development, we now consider different approaches to the discretization of the time dependency of these approximations. Five schemes are considered.

Scheme 1: Explicit centred difference

This is the centred difference scheme (10), where the components of normal velocity are those at the current time and the tangential components of velocity are calculated using (15). The discretization of the viscous term in (7) is also done at the current time. As such, the matrix Q arising from the discretization of the momentum equation is diagonal and contains only a contribution from the temporal term.

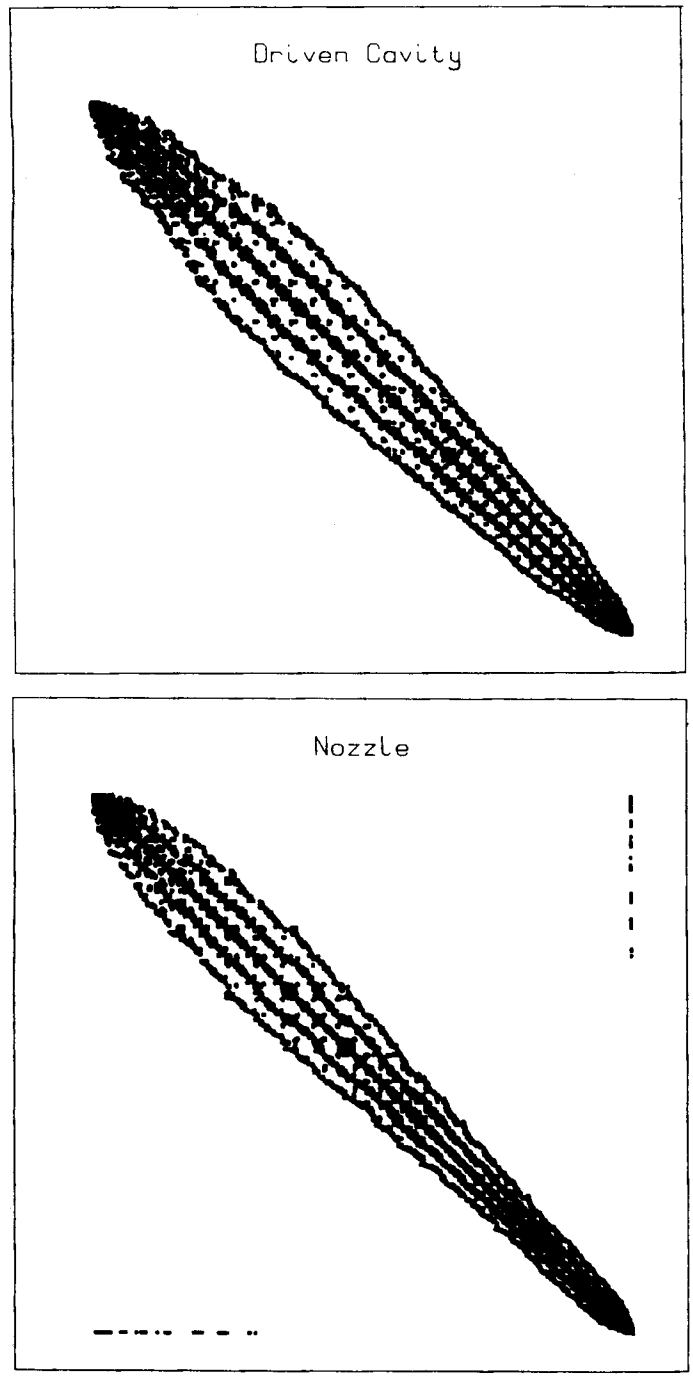

Figure 5. Structure of the dual variable system

Scheme 2: Explicit upwind difference

This is the same as Scheme 1 *except* for that the upwind scheme in (11) is used to approximate the convective term.

Scheme 3: Semi-implicit co-volume integration

This is the scheme used in Reference 4 and is included here primarily as a basis of comparison. The convection term is approximated by area averaging over adjoining triangles:

$$[\nabla(\mathbf{q}\cdot\mathbf{r})]\cdot\mathbf{q}\approx\frac{A_\tau}{A_\sigma+A_\tau}[\nabla(\mathbf{q}\cdot\mathbf{r})]\cdot\mathbf{q}\Big|_\tau+\frac{A_\tau}{A_\sigma+A_\tau}[\nabla(\mathbf{q}\cdot\mathbf{r})]\cdot\mathbf{q}\Big|_\sigma, \tag{22}$$

where A_τ and A_σ are the areas of the triangles¶ τ and σ, and where $\mathbf{r}$ is again a constant unit vector (typically, normal to a triangle's side). Furthermore, since $\nabla\cdot\mathbf{q}=0$,

$$\begin{aligned}[\nabla(\mathbf{q}\cdot\mathbf{r})]\cdot\mathbf{q}|_\sigma=\nabla\cdot[(\mathbf{q}\cdot\mathbf{r})\mathbf{q}]|_\sigma&\approx\frac{1}{A_\sigma}\int_\sigma\nabla\cdot[(\mathbf{q}\cdot\mathbf{r})\mathbf{q}]\,dA\\&=\frac{1}{A_\sigma}\int_{\partial\sigma}(\mathbf{q}\cdot\mathbf{r})(\mathbf{n}\cdot\mathbf{q})\,ds\\&\approx\frac{1}{A_\sigma}\left[\sum_{i=1}^{3}h_i(\mathbf{n}\cdot\mathbf{n}_i)\,\xi_i^{m+1}(\mathbf{q}\cdot\mathbf{r})_i\right],\end{aligned} \tag{23}$$

where $(\mathbf{q}\cdot\mathbf{r})_i=(\xi_i^m\mathbf{n}_i+\eta_i^m\mathbf{s}_i)\cdot\mathbf{r}$, h_i is the length of side i in triangle σ, $\mathbf{n}_i$ and $\mathbf{s}_i$ are unit normal and tangent vectors on this side, and $\mathbf{n}$ is the unit outward normal. The tangential components of velocity η_i^m are determined using (15). Hence, the normal component $\mathbf{q}\cdot\mathbf{n}_i=\xi_i$ is handled implicitly (at time level $m+1$); however, the component of $\mathbf{q}$ in the direction of $\mathbf{r}$, $\mathbf{q}\cdot\mathbf{r}$, is handled explicitly (at time level m). For one-dimensional convection, this is analogous to approximating $(uu_x)^{m+1}$ by $u^{m+1}(u_x)^m$. A more standard approach is to approximate $(uu_x)^{m+1}$ by $u^m(u_x)^{m+1}$. With regard to scheme 3, the analogue of this is to replace ξ_i^{m+1} by ξ_i^m in equation (23) and to approximate $(\mathbf{q}\cdot\mathbf{r})_i$ by $(\mathbf{q}'\cdot\mathbf{r})_i$, where $\mathbf{q}'=\mathbf{q}'_P$, $\mathbf{q}'_Q$, or $\mathbf{q}'_S$ as in (13), evaluated at time level $m+1$. Hence, we write

$$(\mathbf{q}'_i)^{m+1}\equiv\xi_i^{m+1}\mathbf{n}_i+(\eta'_i)^{m+1}\mathbf{s}_i,$$

where $(\eta'_i)^{m+1}$ is approximated by a linear combination of the three normal components of velocity ξ_j^{m+1}, $j=1, 2, 3$. That is, equation (15) is solved, yielding coefficients a_i, b_i and c_i such that

$$(\eta'_i)^{m+1}=a_i\xi_P^{m+1}+b_i\xi_Q^{m+1}+c_i\xi_S^{m+1}.$$

When implemented, this modified scheme 3 gave results that were consistent with the Stokes flow, i.e. the contribution of the convection term was negligible. On closer inspection it is observed that

$$(\mathbf{q}'_i)^{m+1}=\mathbf{q}_\sigma^{m+1}+(\xi_i^{m+1}-\mathbf{q}_\sigma^{m+1}\cdot\mathbf{n}_i)\mathbf{n}_i, \tag{24}$$

where $\mathbf{q}_\sigma^{m+1}$ is the *constant* vector given in (12), evaluated at time level $m+1$, and where we have made use of (14). Further, for all problems considered in this paper, the difference $\xi_i^{m+1}-(\mathbf{q}_\sigma^{m+1}\cdot\mathbf{n}_i)$ was of the order of $10^{-5}\times\xi_i^{m+1}$. That is, $(\mathbf{q}'_i)^{m+1}$ turned out to be a small

¶ We refer to the triangles associated with Voronoi vertices τ and σ as triangles τ and σ.

perturbation of the constant vector $\mathbf{q}_\sigma^{m+1}$. But this implies, referring to (23) and (24), that

$$[\nabla(\mathbf{q}\cdot\mathbf{r})\cdot\mathbf{q}]^{m+1}|_\sigma \approx \frac{1}{A_\sigma}\left[\sum_{i=1}^{3} h_i(\mathbf{n}\cdot\mathbf{n}_i)\,\xi_i^m(\mathbf{q}_i')^{m+1}\cdot\mathbf{r}\right]$$

$$\approx \frac{1}{A_\sigma}(\mathbf{q}_\sigma^{m+1}\cdot\mathbf{r})\sum_{i=1}^{3} h_i(\mathbf{n}\cdot\mathbf{n}_i)\,\xi_i^m \approx 0$$

since the final sum is a representation of the discrete divergence of $\mathbf{q}^m$, and $\mathbf{q}^m$ is discretely divergence-free. So, in fact, the modified scheme 3 yields a negligible effect from the convection term. Note that in the original scheme 3, the tangential components of velocity, η_i^m, are dependent on the normal flow across the sides of triangle σ *and* the normal flows across the sides of the three adjacent triangles (cf. (17)). Apparently, it is this dependency of the tangential velocity components on more than the three normal flows associated with σ that make the original scheme 3 successful. Of course, one could also build this dependency into the modified scheme at the expense of having many more couplings in the equation. We do not pursue this modification further, preferring instead to investigate the use of partially implicit versions of the directional derivative approximations of the convection term developed in Section 2.

Scheme 4: Semi-implicit centred difference

This is the centred difference scheme (10) with normal components of velocity approximated at the new time level, but all tangential components of velocity evaluated at the current time. Hence, in (10), for example,

$$\mathbf{q}_{R'}\cdot\mathbf{n}_P \approx \mathbf{q}_R\cdot\mathbf{n}_P = \xi_R^{m+1}(\mathbf{n}_R\cdot\mathbf{n}_P) + \eta_R^m(\mathbf{s}_R\cdot\mathbf{n}_P).$$

Note that in (10) the distance $|R'-Q'|$ is used.

Scheme 5: Semi-implicit upwind difference

This is the upwind scheme (11) with the same temporal discretization as in scheme 4. Hence, in (11)

$$\mathbf{q}_P\cdot\mathbf{n}_P = \xi_P^{m+1}$$

while, for example,

$$\mathbf{q}_{Q'}\cdot\mathbf{n}_P \approx \mathbf{q}_Q\cdot\mathbf{n}_P = \xi_Q^{m+1}(\mathbf{n}_Q\cdot\mathbf{n}_P) + \eta_Q^m(\mathbf{s}_Q\cdot\mathbf{n}_P).$$

The distances $|P-Q'|$ and $|P-R'|$ are retained in (11).

6. NUMERICAL EXAMPLES

6.1. *Poiseuille flow in a channel*

As a demonstration of the convergence of the new schemes 1, 2, 4 and 5, we consider incompressible flow (unit density) in a channel, $\Omega=[1,4]\times[1,4]$, having no-slip walls parallel to the x-axis. We also assume unit viscosity and a uniform pressure of zero at the exit, $x=4$. At the inlet boundary ($x=1$), we assume a parabolic velocity profile $q_1(1,y)=-(y-1)(y-4)$, $q_2(1,y)=0{\cdot}0$. The true steady-state solution to this problem is

$$q_1(x,y) = -(y-1)(y-4),$$
$$q_2(x,y) = 0{\cdot}0,$$
$$p(x,y) = 8-2x.$$

Table I. Poiseuille flow results

	Number of triangles		
	20	84	358
Size of primitive system	47	198	883
Size of dual variable system	7	36	167
Semi-Bandwidth of dual variable system	5	17	43
Maximum cell side	1·4938	0·7071	0·3535
Scheme 3, co-volume integration			
$\|u_i-\mathbf{q}\cdot\mathbf{n}_i\|_W$	0·2609	0·0660	0·0259
Order α	—	1·84	1·35
Schemes 2 and 5, upwind difference			
$\|u_i-\mathbf{q}\cdot n_i\|_W$	0·2505	0·1395	0·0649
Order α	—	1·27	1·10
Schemes 1 and 4, centred difference			
$\|u_i-\mathbf{q}\cdot\mathbf{n}_i\|_W$	0·2676	0·1223	0·0593
Order α	—	1·04	1·04

Table I contains the results of utilizing schemes 1–6 on 3 meshes obtained by successively decreasing the mesh gage as illustrated in Figure 6. These results were obtained after 10 steps using a step size of 1·0, starting with a null initial condition.

For a mesh function e_i, the norm $\|e_i\|_W$ is defined by $\|e_i\|_W \equiv (\sum_i e_i^2 h_i h_i')^{1/2}$, where h_i' is the length of the ith link and as before h_i is the length of the side of a triangle cut by the ith link. If $H \equiv \max_i h_i$ and $\|e_i^H\|_W = cH^\alpha$, then we estimate the *order of convergence* α, given $\|e_i^H\|$ for two values H_1 and H_2 of H, by

$$\alpha = \frac{\ln(\|e_i^{H_1}\|/\|e_i^{H_2}\|)}{\ln(\|H_1\|/\|H_2\|)}.$$

Estimates of α are given in Table I. In terms of the W-norm, we see that $1 \leq \alpha \leq 2$, which is consistent with the theoretical results in References 7, 15 and 16 since the triangulations are not regular.

6.2. *Driven cavity*

The flow region is a unit square, three sides of which represent no-slip walls ($\mathbf{q}=\mathbf{0}$). The top is an infinite lid sliding to the left with unit velocity. The flow is incompressible (unit density) and the Reynolds number $Re = 1/\nu$ is determined by specifying the viscosity ν.

The cavity is subdivided into 1016 triangles as shown in Figure 7. The associated primitive system has 2501 unknowns, while the dual variable system is 469×469. A uniform time step of 0·005 was used and a steady-state solution was said to be obtained when the maximum change in normal velocity was less than 10^{-3}. For $Re = 400$, Figure 7 also contains comparisons of the dual variable method (using schemes 1–5) with those of Burggraf.[24] The latter is a finite difference solution on a uniform grid with over 3000 unknowns. Note that schemes 1 and 4 gave virtually identical results for the steady-state solutions. This is also true of schemes 2 and 5.

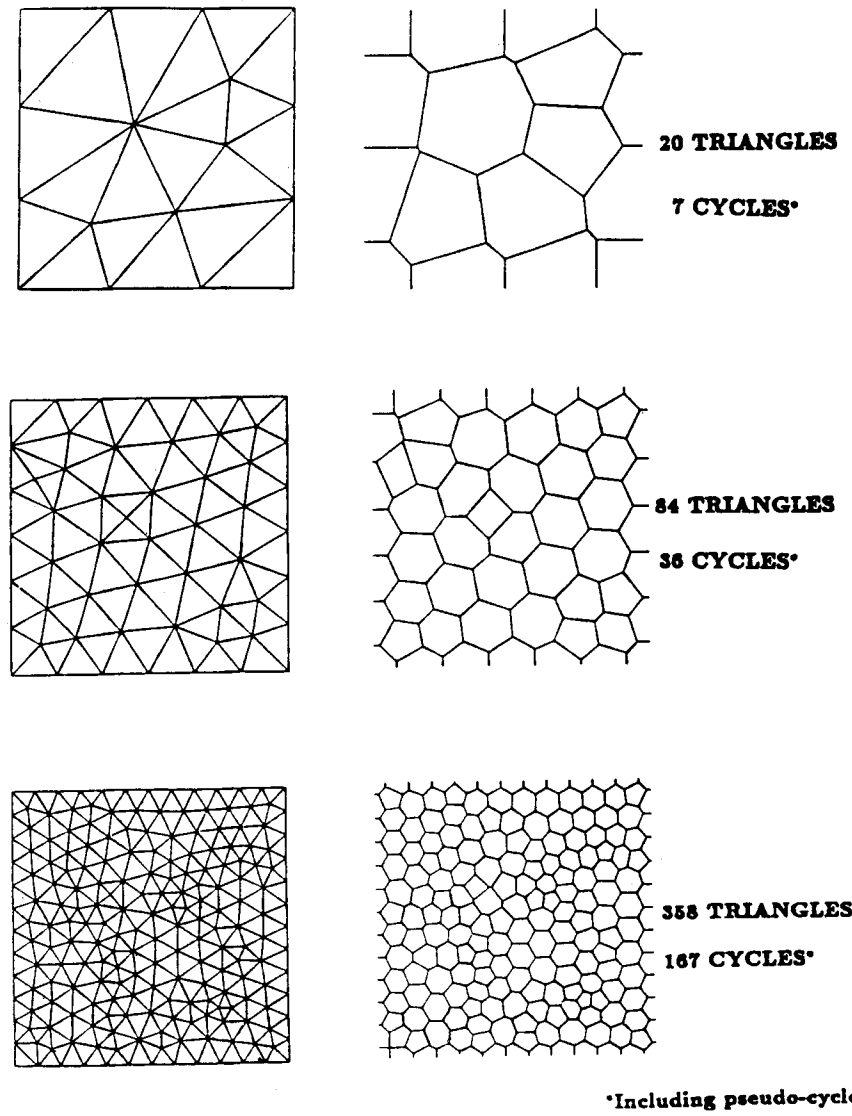

Figure 6. Three triangulations of the channel

For this problem ($Re = 400$), increasing the time step to 0·5, 0·6, 1·5, and 4·0 for schemes 1, 2, 3, and 4, respectively produces velocities of the order of 10^6. Hence, these schemes impose stability conditions on the time step. In contrast, the steady-state solution using scheme 5 and a time step of 10·0 is virtually identical to that shown in Figure 8. In fact, using scheme 5, similar results are obtained with a time step of 10^3. This and other numerical evidence supports the conclusion that scheme 5 (the semi-implicit upwind scheme) is unconditionally stable.

Increasing the Reynold's number also gave unstable results when scheme 3 was used. For example, a time step of 0·1 and $Re = 4000$ ($\nu = 0{\cdot}00025$) resulted in unstable calculations. However, the upwind scheme remained stable for $Re = 4000$ and a time step of 10·0. The velocity field for the upwind scheme is given in Figure 8 for a time step of 1·0.

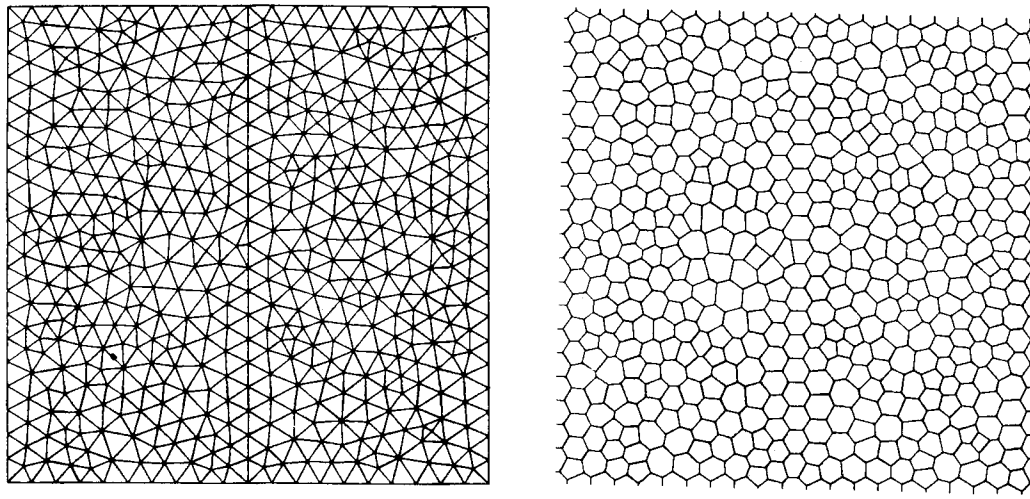

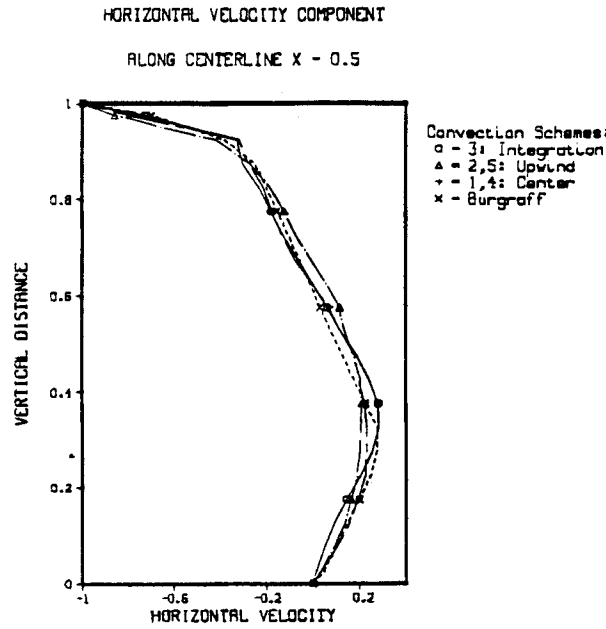

Figure 7. Comparisons of centreline velocities for a driven cavity ($Re = 400$)

6.3. *Flow past a circular cylinder*

Figure 9 shows a triangulation of the channel $[0, 1{\cdot}5] \times [0, 1]$ containing a circular obstacle of radius 0·1 centred at (0·5, 0·5). This triangulation consists of 586 triangles and 315 vertices. The dual tessellation of Voronoi polygons (including boundary tiles) is also given in Figure 9.

A unit normal velocity is specified on the boundary segment $x = 0, 0 \leq y \leq 1$, and a unit pressure on the segment $x = 1{\cdot}5, 0 \leq y \leq 1$. On the boundary segments $y = 0$ and $y = 1$, the velocity $\mathbf{q} = (1, 0)$ is specified, and the boundary of the obstacle is assumed to be no-slip ($\mathbf{q} = \mathbf{0}$). The viscosity was

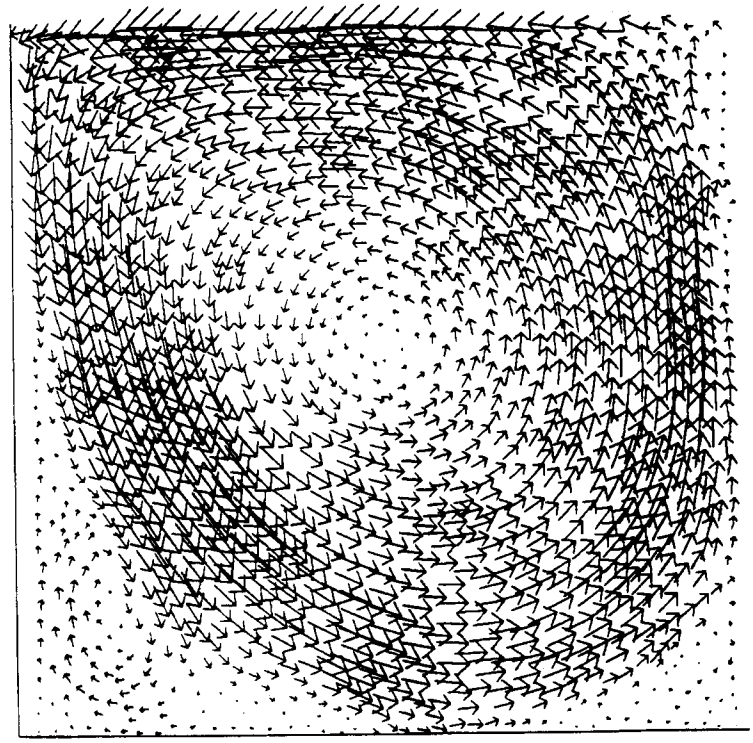

Figure 8. Velocity field ($Re = 4000$): upwind scheme

chosen to be 0·002, which corresponds to a Reynold's number of 100 (relative to the diameter of the obstacle). The network **N** consists of the 857 links (sides of the 272 tiles which are closed Voronoi polygons) and the 586 nodes (circumcentres of triangles). There are also four boundary links to the pressure-specified nodes.

The primitive system has dimension 1447 ($=857+4+586$), while the dual variable system has dimension 275 ($=857+4-586$). This is a reduction by a factor of 5·3 in the size of the system to be solved at each time step.

Schemes 3 and 5 were used with success for this problem with a time step of 0·005. However, scheme 3 (the co-volume integration scheme) gives unstable results when this time step is increased to 0·05. In contrast, the upwind scheme (scheme 5) remains bounded even for time steps larger than 1·0. Figure 10 illustrates typical plots of the streamlines for various values of time when the upwind scheme is used. Vortices are formed beyond the obstacle and are persistently shed downstream.

6.4. Flow in a nozzle section at high incidence

The geometry of this problem is based on the cross-section of a nozzle similar to that studied by Glowinski and Periaux[25] and is shown in Figure 11; see also Reference 26. The primary intent in presenting this example is to illustrate the ability of the method to deal with a multiply connected flow region containing more than a single obstacle; in this case the two side-walls of the nozzle.

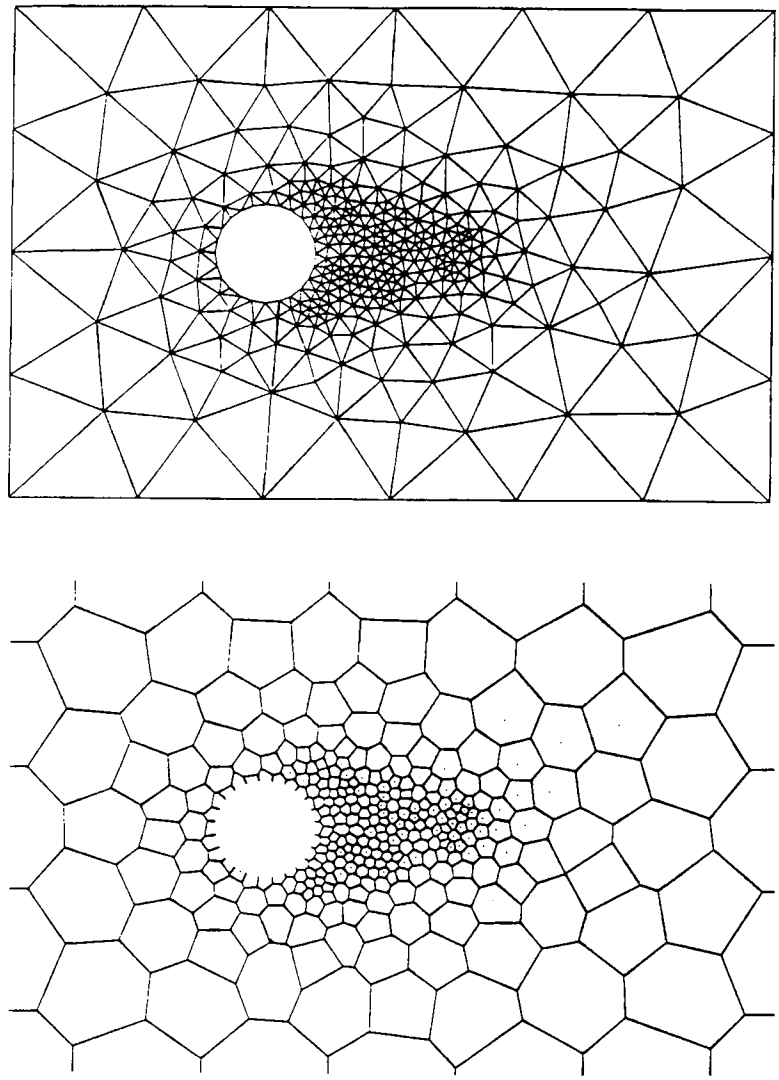

Figure 9. Delaunay and Voronoi tessellations for a channel with a circular obstacle

A free stream enters at the right boundary and impinges on the side-walls of the nozzle at 40°. The Reynolds number, which is based on the free-stream velocity and the distance between the two walls of the nozzle inlet, is 750. A constant pressure is applied along the length of the downstream boundary. In contrast to the work presented in Reference 25, we do not attempt to simulate a suction effect due to the engine by prescribing a given flux on a cross-section of the inlet. A time step of 0·01 was used in conjunction with the upwind scheme (scheme 5) for the convection term. The computations show that vortices form behind the side-walls and are shed in a periodic manner. See Figure 12 for samples of the instantaneous streamline distribution in the vicinity of the nozzle.

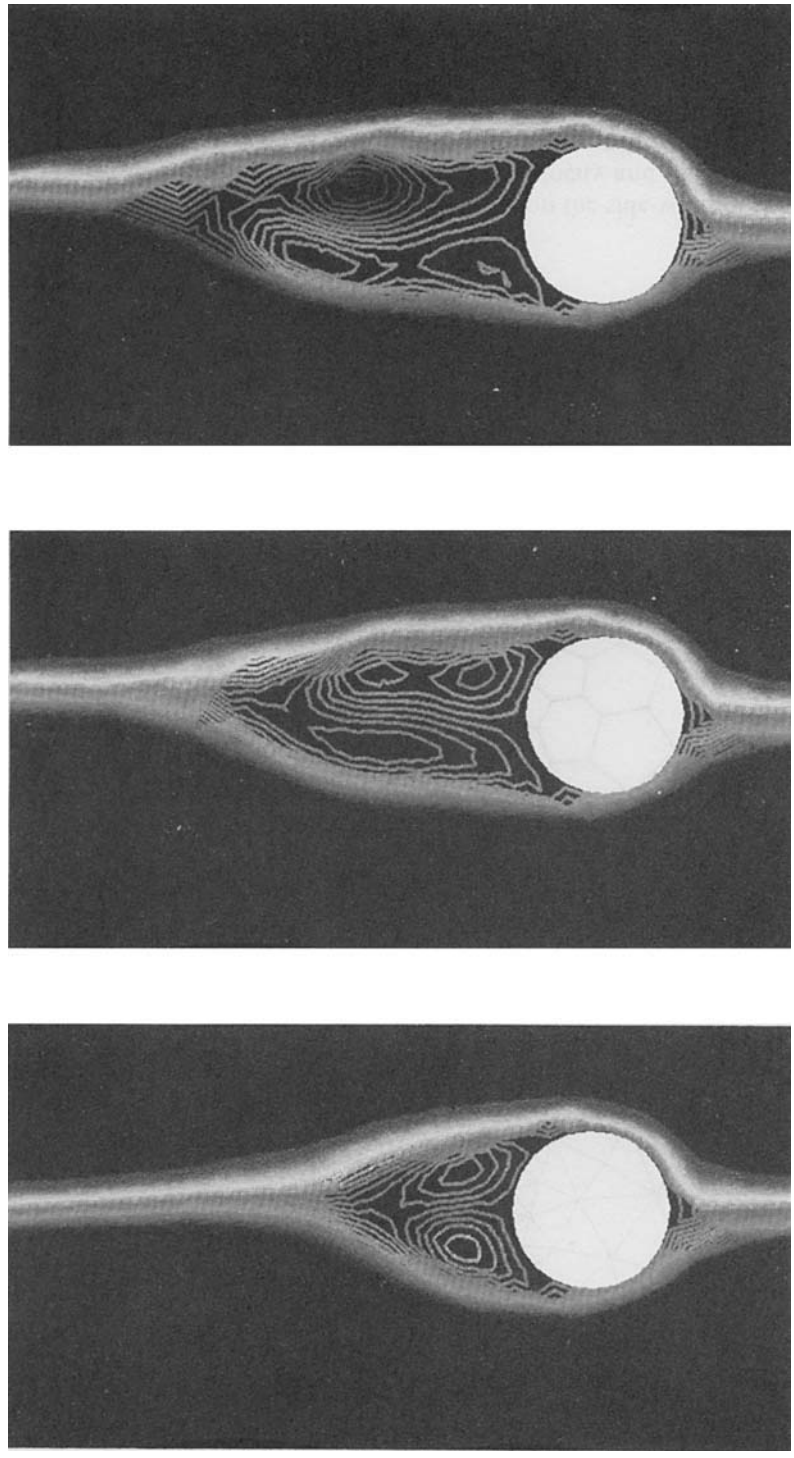

Figure 10. Streamlines of flow past a circular obstacle ($Re = 100$): upwind scheme

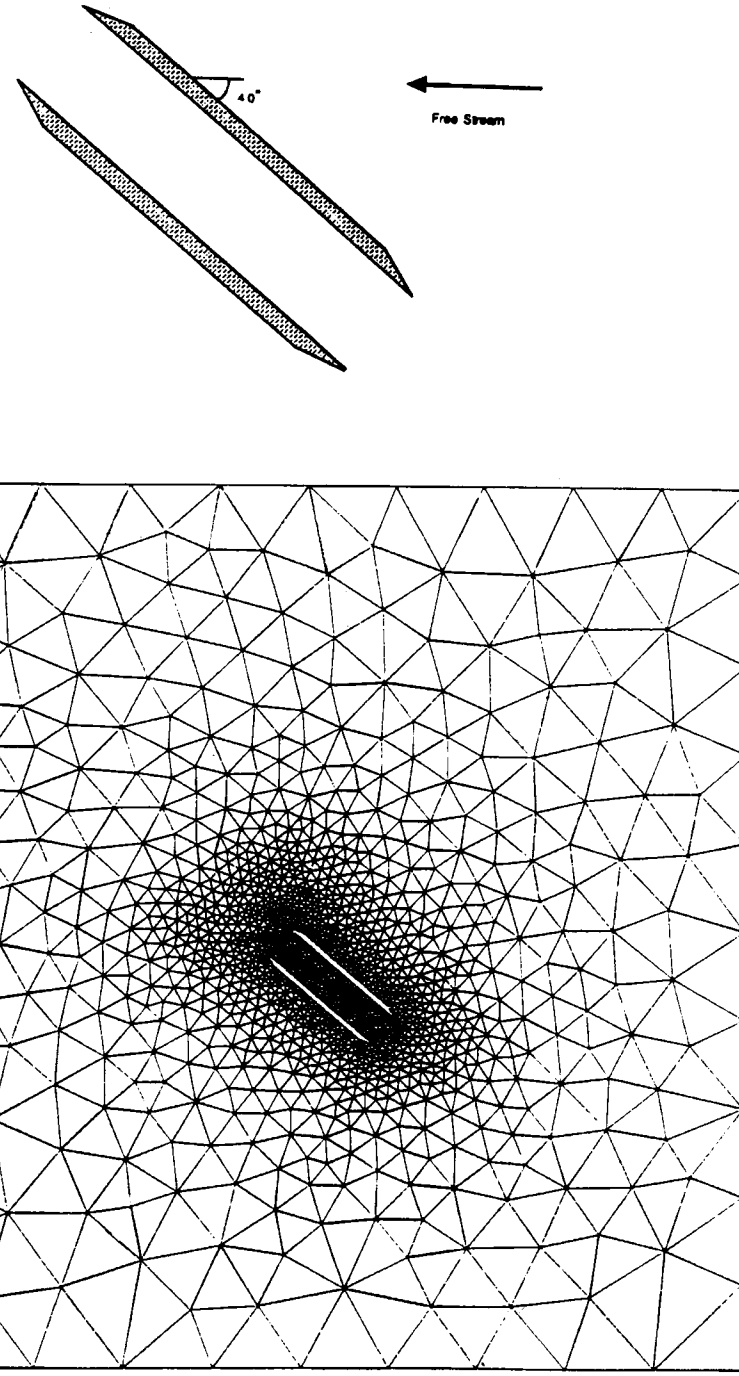

Figure 11. Glowinski's nozzle

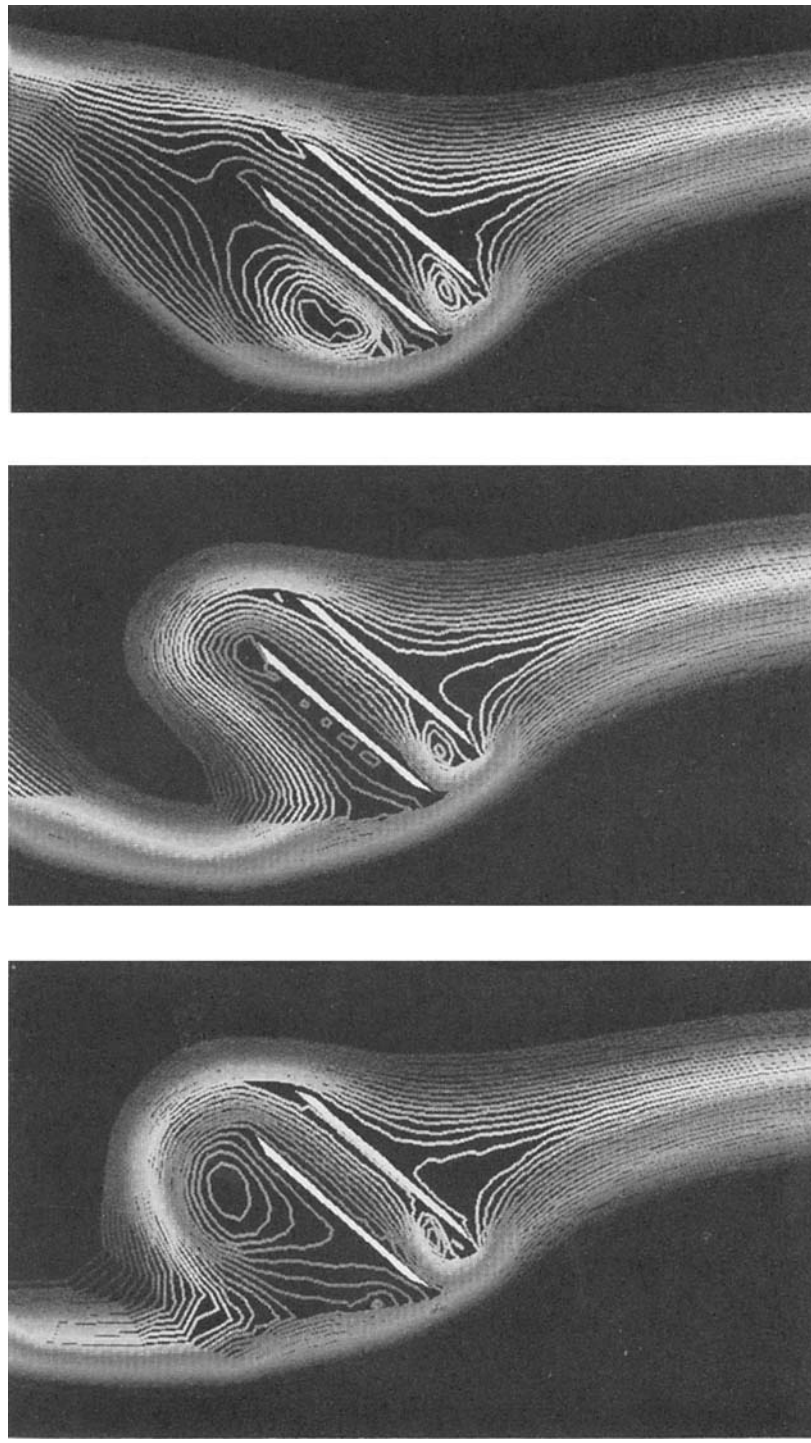

Figure 12. Streamlines for the nozzle: upwind scheme

There were 2252 triangles and 1194 polygonal tiles in the decomposition of the flow region, and the network **N** contained 3318 links. The primitive system was 5570×5570, while the dual variable system was 1066×1066, yielding a reduction factor of 5·4.

7. CONCLUSIONS

Numerical solutions of flow problems are often facilitated by the use of triangular grids. The equations of incompressible flow can be discretized on the triangular cells of such a grid by applying a co-volume technique. While the treatment of the continuity equation is straightforward, more care is required with the vector momentum equation. A co-ordinate-free scalar equation can be deduced from the momentum equation in which the convection, viscous stress, and pressure gradient terms appear as directional derivatives. This allows these terms to be approximated in a manner that is compatible with the co-volume methodology. In particular, centred and upwind forms of the convection term occur in a completely natural way. The overall discrete system gives the node laws and link characteristics of a directed network defined by the Voronoi polygons associated with the triangles. Utilizing a transformation related to the dual network, one can obtain an equivalent system that is about one-fifth the size of the original. Computations involving a variety of problems and geometries show that these network methods produce numerical solutions comparable in accuracy to those of the more conventional techniques on rectangular grids.

ACKNOWLEDGEMENTS

Work performed under the auspices of the U.S. Department of Energy contract number DE-AC07-76-IDO1570, supported in part by the INEL Long-term Research Initiatives Program.

REFERENCES

1. S. H. Chou, 'A Network model for incompressible two-fluid flow and its numerical solution', *Numer. Methods Part. Diff. Eq.*, **5**, 1–24 (1989).
2. T. A. Porsching, 'A network model for two-fluid, two-phase flow', *Numer. Methods Part. Diff. Eq.*, **1**, 295–313 (1985).
3. S. Choudhury and R. A. Nicolaides, 'Discretizations of incompressible vorticity–velocity equations on triangular meshes', *Int. j. numer methods fluids.*, (to appear).
4. C. A. Hall, J. C. Cavendish and W. H. Frey, 'The dual variable method for solving fluid flow difference equations on Delaunay triangulations', *Comput. Fluids*, **20**, 145–164 (1991).
5. R. A. Nicolaides, 'Flow discretization by complementary volume techniques', AIAA paper 89-1978, *Proc. 9th AIAA CFD Meeting*, Buffalo, NY, June 1989.
6. R. A. Nicolaides, 'Triangular discretization for the vorticity–velocity equations', *Proc. 7th Intl. Conf. Finite Elements in Flow Problems*, Huntsville, AL, 1989.
7. R. A. Nicolaides, 'Direct discretization of planar Div–Curl problems', *SIAM J. Numer. Anal.*, **29**, 32–56 (1992).
8. F. H. Harlow and F. E. Welch, 'Numerical calculations of time dependent viscous incompressible flow of fluid with a free surface', *Phys. Fluids*, **8**, 2182–2189 (1965).
9. D. F. Watson, 'Computing the *n*-dimensional Delaunay tessellation with applications to Voronoi polytopes', *Comput. J.*, **24**, 167–172 (1981).
10. C. Berge and A. Ghouila-Houri, *Programming, Games and Transportation Networks*, Methuen, London, 1965.
11. R. Amit, C. A. Hall and T. A. Porsching, 'An application of network theory to the solution of implicit Navier–Stokes difference equations', *J. Comput. Phys.*, **40**, 183–201 (1981).
12. C. A. Hall, 'Numerical solution of Navier–Stokes problems by the dual variable method', *SIAM J. Alg. Disc. Methods*, **6**, 220–236 (1985).
13. K. Gustafson and R. Hartman, 'On the dimension of a finite difference approximation to divergence-free vectors', in K. Gustafson and W. Rheinboldt (eds), *Quantum Mechanics in Mathematics, Chemistry and Physics*, Plenum Press, New York, 1981, pp. 125–131.
14. K. Gustafson and R. Hartman, 'Graph theory and fluid dynamics', *SIAM. J. Alg. Disc. Methods*, **6**, 643–656 (1985).
15. R. A. Nicolaides and X. Wu, 'Numerical solution of the Hamel problem by a covolume method', in W. G. Habashi and M. Hafez (eds.), *Advances in CFD*, (to appear).

16. X. Wu, 'Analysis and applications of the covolume method for the Navier–Stokes equations', *Ph.D. Dissertation*, Carnegie-Mellon University, 1991.
17. R. Peyret and T. D. Taylor, *Computational Methods for Fluid Flow*, Springer, Berlin, 1983.
18. W. H. Frey and J. C. Cavendish, 'Fast planar mesh generation using the Delaunay triangulation', General Motors Research Publication, GMR-4555, 1983.
19. A. Segal, 'The implementation of boundary conditions of the type u equals unknown constant in finite element codes', *Commun. Appl. Numer. Methods*, **1**, 71–80 (1985).
20. I. S. Duff, A. M. Erisman and J. K. Reid, *Direct Methods for Sparse Matrices*, Oxford Science Publications, Clarendon Press, Oxford, 1986.
21. J. M. Doster and M. B. Richards, 'Parallel processing algorithms for the finite difference solution to the Navier–Stokes equations', *Nucl. Sci. Eng.*, **93**, 69–77 (1986).
22. G. L. Mesina, 'A parallel algorithm for solving linear equations arising from one-dimensional network problems', *Proc. ANS Intl. Top. Meeting on Advances in Math., Comp. and Reactor Phys.*, Pittsburgh, PA, May, 1991.
23. T. A. Porsching, J. H. Murphy and J. A. Redfield, 'Stable numerical integration of conservation equations for hydraulic networks', *Nucl. Sci. Eng.*, **43**, 218–225 (1971).
24. O. R. Burggraf, 'Analytical and numerical studies of the structure of steady separated flows', *J. Fluid Mech.*, **24**, 113–151 (1966).
25. R. Glowinski and J. Periaux, 'Finite element least squares and domains decomposition methods for the numerical solution of nonlinear problems in fluid dynamics', in F. Brezzi (ed), *Numerical Methods in Fluid Dynamics, Como 1983*, Springer, Berlin, 1985.
26. R. Glowinski, 'Viscous flow simulations by finite element methods and related numerical techniques', in E. M. Murman and S. S. Abarbanel (eds.), *Progress and Supercomputing in Computational Fluid Dynamics*, Birkhauser, Boston, 1985.